

# Influence of Processing Induced Morphology on the Performance of PP Injected Intricate Pieces Modified with MWCNT as a Painting Aide

Alejandra Costantino<sup>1</sup>, Leandro Ramajo<sup>1</sup>, Julio Viana<sup>2</sup>, Caren Rosales<sup>1</sup>, Antonio Pontes<sup>2</sup>, Valeria Pettarin<sup>1</sup>, 

<sup>1</sup>Institute of Materials Science and Technology (INTEMA), CONICET-University of Mar del Plata, Colón 10850, 7600 Mar del Plata, Argentina

<sup>2</sup>Institute for Polymers and Composites (IPC/I3N), University of Minho, Campus de Azurém, 4800-058 Guimaraes, Portugal

\*Corresponding author: E-mail: pettarin@fi.mdp.edu.ar; Tel.: (+54) 9 223 5013624

DOI: 10.5185/amlett.2021.041618

Carbon nanotubes are currently added to polymers to avoid extra-stages in the electrostatic painting process. However, the attained particle network after processing a final part could affect the mechanical properties and thermal stability of nanocomposites. It is then important to evaluate not only the functional properties, but also the overall performance of these pieces. In this work, boxes of polypropylene (PP) modified with multi-walled carbon nanotubes (MWCNT) were injection molded. Morphology induced by processing was characterized at different locations of the moldings to correlate the influence of in-homogeneities and flow pattern with the overall performance of the molded boxes. PP/MWCNT presented a better aesthetic quality and a markedly better thermal stability than pure PP. It was confirmed that the nanocomposite has high dielectric permittivity, low dielectric losses and relatively good DC conductivity. Regarding mechanical properties, MWCNT induced a slight improvement in flexural elastic modulus. Although fracture initiated at practically the same loading levels for both materials, the propagation energy was deteriorated by MWCNT presence. Differences in both electrical and mechanical behavior were found through the PP/MWCNT pieces as result of distinct MWCNT orientation and distribution. It was then concluded that processing has a great influence on parts performance.

## Introduction

From an industrial point of view, final polymeric products should meet both certain structural requirements and adequate aesthetic quality. Produced parts are commonly subjected to different surface finishing techniques to achieve desired aesthetic requirements, being the electrostatic painting (e-painting) the most efficient technique. E-painting offers great economic, environmental and aesthetic advantages, among the high reduction of used paint and volatile emissions, as the most relevant [1]. However, this technique cannot be directly applied in polymers due to their insulating properties. Plastic parts need to be previously prepared by painting them with a primer, adding a further stage to the production cycle. Alternatively, and to avoid this extra step, a painting agent (e.g., a conductive filler) could be added to the polymer during manufacturing stage to modify its electrical properties and make it suitable to be directly electrostatic painted.

Polymer/MWCNT nanocomposites have attracted much attention due to the great electrical properties achieved with a low weight nanofiller concentration. In the automotive industry, MWCNT are already being used as a conducting agent to aid in e-painting [2,3]. In fact, one of the first applications which brought nanocomposites to

commercial status was to add MWCNT to a resin as electrostatic painting aid [4]. Moreover, conductive polymers have antistatic properties, which have aroused much attention from industrial fields, due to the reduction in static electricity that can damage electronics devices, ignite flammable fumes and interfere with radio navigation in aircrafts [5].

Due to their very high aspect ratio – often in the range of 100 to 1000 – MWCNT are able to form an effective conductive pathway in polymer composites at lower volume fraction than carbon black or carbon fiber [5]. The electrical conductivity of polymer-MWCNT composites is known to be dependent not only on the diameter, length, specific surface area and surface conductivity of the MWCNT; their dispersion and interaction with the polymer matrix; but also, on the percolation threshold. In the case of PP based composites, the electrical percolation threshold is reached at about 10–20 wt.% with carbon black [6], and at only 1–2 wt.% with MWCNT [3,5,6], or even less [7,8]. Differences in the percentage needed for percolation threshold are attributed to different CNT orientations [9–11]. L.J. Lanticse *et. al.*, demonstrated that when some preferred orientation exists, the percolation threshold increases due to the lower probability for these fillers to be in contact with each other [12].

It is important to point out here that most of the composites parts based in thermoplastic polymers are mainly fabricated via injection molding. This technique induces some inherent defects as flux marks and weld lines which may compromise aesthetic properties as well as integrity of injection molded parts. Moreover, and very relevant, it is known that injection molding induces the orientation of polymer molecules and particles [13,14]. Use of MWCNT requires an understanding of how processing conditions influence nanocomposite properties. Besides, as the percolation threshold strongly depends on the MWCNT orientation, dispersion and distribution, this is especially important in injected parts since they will be strongly affected by the thermo mechanical complex field developed during processing [15-17]. It has been reported that injection-molded parts have a higher percolation threshold – around 3% – than compressed ones due to the morphology developed during the processing, characterized by a preferential alignment of particles along the flow direction [13,18,19]. Moreover, inhomogeneities such as weld lines are present in almost all commercial injected parts.

Considering this, it is striking that they are not enough analyzed in literature, when referred to CNT modified injected polymers. Most works deal with normative specimens or simple one gated injected pieces with no edges or weld lines. There are plenty of works dealing with PP/CNT composites [20-25], but only few taking into account the influence of processing, and they do not analyze actual final pieces. For example, Villmow *et. al.*, studied the influence of injection molding parameters on the electrical resistivity of polycarbonate filled with 2 and 5% of multiwalled carbon nano tubes injected pieces [26]. They found differences in resistivity values locally within the injected plates of five orders of magnitude due to the flow pattern developed during processing. However, their pieces were only one gated injected without weld lines or typical injection inhomogeneities. Wu *et. al.*, studied mechanical and electrical properties of injection-molded carbon nanotube-filled PET/PVDF blends [27], but they also injected simple geometries. Arjmand *et. al.*, showed in their study that mold designs and processing conditions significantly influence the electrical conductivity and shielding behavior of injection molded CNT-filled composites, however they didn't work with real representative pieces [18]. Abbasi *et. al.*, investigated the effect of flow field and deformation rate on the nanotube alignment and on the rheological, electrical and mechanical properties of PC/multiwalled carbon nanotube nanocomposites [28]. They found that orientation developed during processing is determinant of those properties, but they evaluated the performance of simple one gated injected disc and bars with no real defects.

The challenge of adding these particles to a thermoplastic matrix is to obtain a composite with improved functional properties without sacrificing the mechanical and rheological properties required by the automotive market. The particle network could affect the mechanical properties and thermal stability of nanocomposites, because nanotubes restrict the polymer

chain mobility of the matrix. It is therefore clear the need to evaluate not only the functional properties, but also the mechanical performance of this type of injected pieces.

In this work, the feasibility of obtain PP actual injected complex pieces with good electrostatic painting ability without compromising mechanical performance is explored. To this aim, double gated box-like moldings of PP modified with MWCNT were injected. Due to the gating options (2 pin gates), the major box surface shows a central weld-line, originated by the top-to-top meeting of the two flow fronts. Morphology induced by processing was characterized at different locations (weld line and injection point zones) in the moldings to assess the influence of inhomogeneities and flow pattern upon the dielectric and mechanical behavior. Dielectric measurements were performed as a function of frequency in order to understand the relaxation process and relate it with the microstructure. In addition, AC and DC electrical conductivity was investigated. Thermal, mechanical and fracture performance were also characterized. Finally, a correlation between processing, painting efficiency and mechanical performance is presented.

## Experimental

### *Materials, blends compounding and processing*

Polypropylene (PP) homopolymer powder from DUCOR 3048 TC with specific gravity of 0.9 g/cm<sup>3</sup> and a melt flow index MFI=48 g/10 min (190°C, 2.16 kg; a high MFI was chosen to avoid the excessive viscosity of the blend) was selected. Commercial multi-walled carbon nanotubes (MWCNT) NANOCYLTM NC7000 (9.5 nm diameter and 1.5 μm length, recommended by manufacturer for electrostatic dissipative applications) were used.

It is pointed out in literature that a balancing effect seemed to occur for PP materials containing up to 3.7 vol.% of not functionalized CNT [29]. Moreover, the percolation threshold required to induce electrical conductivity is achieved between 2-3% in the case of oriented pieces (as injected ones) [12]. Thus, an incorporation of 3% of MWCNT on PP was chosen. In general, the compatibility between CNT and polymer matrices, especially non-polar ones like polyolefins, is limited by the remarkable tendency of the former to agglomerate, leading to mean defect sites in the composites and compromising their efficiency in “reinforcing” the polymer matrices. The dispersion is usually hindered by their large aspect ratio and strong Vander-Waals attractions between CNT, such that commercial products are always available as severely entangled nanotubes [30]. To favor the dispersion of MWCNT, polypropylene grafted maleic anhydride (PP-g-MA) 427945 from Sigma-Aldrich was added as compatibilizer.

Neat PP and PP/MWCNT/PP-g-MA (95.5/3/1.5% w/w) were injected as box-like parts. In the case of the nanocomposite, a MWNTs/PP/PP-g-MA masterbatch (10/88.5/1.5% w/w/w) was compounded in a twin-screw micro extruder prior to injection. Two gated boxes of dimensions: 152 mm width, 73 mm length, 16 mm height

and 1,6 mm thick were processed in an injection molding machine Ferromatik-Milacron K85 (Injection temperature = 190°C; mold temperature = 60°C; injection speed = 30 mm/s; injection pressure = 58 bar; injection time = 1.29 s; packing pressure = 25 bar; packing speed = 30 mm/s; packing time = 5 s; cooling time = 30 s).

### Part shrinkage measurements

The shrinkage ( $S$ ) of moldings was measured on a minimum of three specimens for each condition and in four different zones of the samples: three measurements in the width ( $W$ ) and one in the length ( $L$ ). Measurements were done after 24 hours of parts processing with a digital caliper. Parts were stored in controlled temperature and humidity conditions. Shrinkage indexes were determined using the following equations:

$$S_L = \frac{l_M - l}{l_M}, \quad S_W = \frac{w_M - w}{w_M} \quad (1)$$

where  $l$  and  $w$  refers to the length and width of the part;  $l_M$  and  $w_M$  represents the mold cavity dimensions.

### Morphology

Morphology and microstructure developed in the injected boxes were evaluated in two zones of interest according to Fig. 1(a) by using combined structure sensitive techniques.

Polarized light microscopy (PLM) was used to observe the microstructure of the moldings through the thickness. 15  $\mu\text{m}$  thick samples were cut with a Leitz 1401 microtome, placed between glass lamina with a liquid of matched refractive index, and observed with an Olympus BH2 polarized light microscope.

Fracture surfaces of samples were analyzed using a JEOL JSM-6460LV scanning electron microscope (SEM) at an accelerating voltage of 20 kV. Samples were previously sputter coated with a thin layer of gold before they were observed.

Transmission electron microscopy (TEM) photographs were obtained with a Jeol 100 CX microscope using an acceleration voltage of 200 kV. Samples were ultramicrotomed at room temperature with a diamond knife to a 70 nm thick cross section.

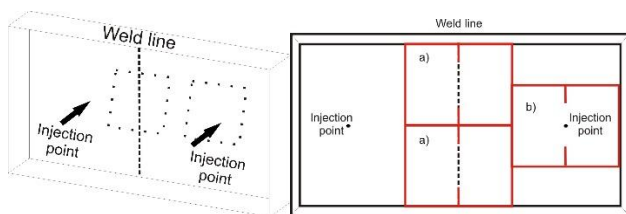


Fig. 1. Scheme of boxes and (a) location of zones of interest (point lines); (b) fracture samples as cut from the injected boxes including weld line and including injection point.

### Rheological measurements

Dynamic oscillatory shear rheological behavior was evaluated by using an AntonPaar, Physica MCR-301 instrument in parallel-plate geometry with a diameter of 25 mm, at 190°C. Measurements were performed with

shear stress amplitude,  $\gamma$ , of 0.1% and within frequency range of 0.01-100 Hz.

### Thermal performance

Thermogravimetric analysis (TGA) was carried out in a Shimadzu electrobalance. Experiments were conducted at a constant rate of 10°C.min<sup>-1</sup> from room temperature to 650°C, in air flow, i.e. oxidative atmosphere. About 2 mg of material was loaded into the container. The degradation onset temperature  $T_{0.1}$ , at which 10% degradation occurs, the midpoint degradation temperature  $T_{0.5}$  and the fraction of non-volatiles that remains at 600°C were extracted from the mass loss in the TGA curves while the maximum decomposition temperature ( $T_{max}$ ) was obtained from the derivative thermogravimetric (DTG) curves.

### Electric characterization

The electric and dielectric properties of PP and PP/MWCNT were analyzed at room temperature. The samples, with 1.2 mm thick and 10x10 mm, were taken from the weld line and near to the gate point zones of the injected boxes (Fig. 1a), using a commercial computer numeric control (CNC) machine Sinoco 3030.

For the electrical measurements, commercial silver paste electrodes were coated on both sides of the samples. Dielectric properties were determined using an impedance analyzer Hewlett Packard HP4294A in the frequency range 100 Hz to 1 MHz. Electric resistance ( $R_V$ ) was measured at room temperature using a digital supermegohmmeter Hioki DSM 8104, while electrical conductivity (DC) was determined according to:

$$\sigma_{dc} = \frac{tR_V}{A} \quad (2)$$

where  $t$  and  $A$  are the thickness of the specimen and the effective area of the measuring electrode, respectively.

To complete the electrical behavior characterization of the injected samples, an AC-conductivity analysis was performed. From the imaginary permittivity  $\epsilon''$  values at different frequencies,  $f$ , the AC-conductivity ( $\sigma_{ac}$ ) data can be calculated according to:

$$\sigma_{ac} = \epsilon'' \epsilon_0 \omega \quad (3)$$

being the permittivity of free space  $\epsilon_0 = 8.85 \times 10^{-12}$  F/m and the angular frequency  $\omega = 2\pi f$

### Mechanical and fracture performance

Conventional mechanical properties were determined by means of flexural tests, according to ASTM D 790-3 using a universal testing machine Instron 4467 at 8.5 mm/min, performing at least 5 tests. Flexural modulus of elasticity ( $E_b$ ) was estimated from the slope of the load-deformation curve in the linear range, as:

$$E_b = \frac{L^3 m}{4bd^3} \quad (4)$$

where  $L$  is the span,  $b$  and  $d$  the width and the thickness of the sample, and  $m$  the slope of the tangent to the linear part of load-displacement curve.

Fracture characterization was carried out on mode I double edge-notched tensile specimens (DENT) cut from the moldings (nominal width,  $W$ , of 30 mm, nominal crack to depth ratio,  $a/W$ , of 0.5, and nominal length,  $S$ , of 70 mm), at a crosshead speed of 2 mm/min and room temperature in an Instron 4467 universal testing machine. Sharp notches were introduced by scalpel-sliding a razor blade having an on-edge tip radius of 13  $\mu\text{m}$  with a Ceast Notchvis notching machine. In order to assess influence of the molding singularities (as flow pattern and weld lines) in fracture, DENT samples were cut from different places of the moldings as depicted in **Fig. 1(b)**.

The initiation fracture toughness was evaluated as the stress intensity factor at 5% non-linearity [31]. The load at crack initiation  $F_q$  was determined as the intercept between the load curve and the  $C+5\%$  compliance line,  $C$  being the initial compliance of the load-displacement curve. The stress intensity factor at initiation,  $K_{Iq}$  was then determined as:

$$K_{Iq} = \frac{F_q}{B\sqrt{\frac{W}{2}}} f\left(\frac{a}{W}\right) \quad (5)$$

where  $B$  is the thickness of the sample,  $W$  is the width of the sample,  $a$  is the length of the notch, and  $f(a/W)$  is the function of the notch to width that for DENT samples is:

$$f\left(\frac{a}{W}\right) = \frac{\sqrt{\pi a}}{\sqrt{1-\frac{a}{W}}} \left[ 1.122 - 0.56\left(\frac{a}{W}\right) - 0.205\left(\frac{a}{W}\right)^2 + 0.471\left(\frac{a}{W}\right)^3 + 0.19\left(\frac{a}{W}\right)^4 \right] \quad (6)$$

In addition to the stress intensity factor at initiation, the propagation value of the strain energy release rate,  $G_{cp}$ , was estimated from the total fracture energy,  $U_{tot}$ , as [32]:

$$G_{cp} = \frac{U_{tot}}{B(W-a)} \quad (7)$$

Fracture surfaces of broken samples were analyzed using a JEOL JSM-6460LV scanning electron microscope (SEM) at an accelerating voltage of 20 kV. Samples were sputter coated with a thin layer of gold before they were observed.

## Results and discussion

### Moldings characteristics

Macroscopic views of the moldings indicated that the presence of MWCNT decreases boxes warpage (**Fig. 2a**). Consistently, the shrinkage of PP/MWCNT boxes are 33% and 50% smaller in longitudinal and transversal directions respectively, indicating that PP/MWCNT parts are the ones with higher final quality (**Fig. 2b**). Several authors have also seen this reduction in warpage with nanofillers [4,33]. It has been proposed that nanofillers favor the nucleation instead of crystal growth during the crystallization process, i.e. giving place to smaller spherulites in injection-molded parts. This limits the local differential shrinkage and therefore the parts warpage. Another reason for the warpage reduction noticed upon MWCNT addition may also be that the higher the rigidity of the material is, the less the part is able to deform. A weld line is easily seen at naked eye in the center of PP/MWCNT injected boxes. Morphology studies in next section will aid to the understanding of this feature.

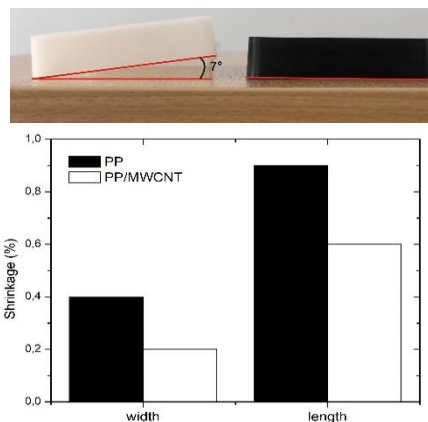


**Fig. 2.** Boxes aesthetic characteristics: lateral view of injected boxes and their shrinkage.

### Morphology and microstructure

**Fig. 3** shows cross sections of injected parts between injection gates that contain the weld line observed by PLM. Two different zones can be recognized: one zone near the injection gates (governed by lubrication hypothesis, which implies zero velocity component in the thickness direction) and characterized by a multi-layer structure; and another zone characterized by a quasi-parabolic shaped advancing flow front (governed by a fountain flow, which implies the presence of a through-the-thickness velocity component). It has been proposed in literature that the multilayer structure of the first zone is due to particles orientation due to the thermo-mechanical profile to which they are exposed during processing [34].

SEM and TEM photographs show both agglomerated and fully dispersed CNT (**Fig. 3(b)** and **3(c)** respectively). CNT agglomerates are oriented in the flow direction in the injection gate region. Moreover, an orientation profile of the MWCNT through the molding thickness is observed in this region: particles in skin zone are preferentially oriented with its longitudinal axis parallel to the advancing flow front (within the agglomerates and at individual level), while in the core zone they tend to align transversally, as would be expected for a fiber reinforced polymer [4,35]. It is known that elongational flow is especially relevant near the injection point, this "shear/elongation" phenomenon across the thickness being the responsible of the differences in the orientation levels between the skin and the core regions.

Regarding the weld line region, agglomerates seem to be more diffuse and there is no preferential orientation of MWCNT both in the skin and core zones. On the contrary, in the advancing flow front the lubrication approach is no longer valid, and reinforcements are aligned randomly due to the three-dimensional nature of this flow, which drives the reinforcement toward the skin passing through the fountain flow. Upon meeting, particles in these two flow fronts do not have enough time to align before "freeze" in the polymer as a result of cooling. In summary, the heterogeneous nature of the weld line is mainly due to the anisotropic orientation of the particles and polymer molecules in this area. In order to gain clarity, all these features of nanocomposite's morphology are schematized in **Fig. 3(d)**.

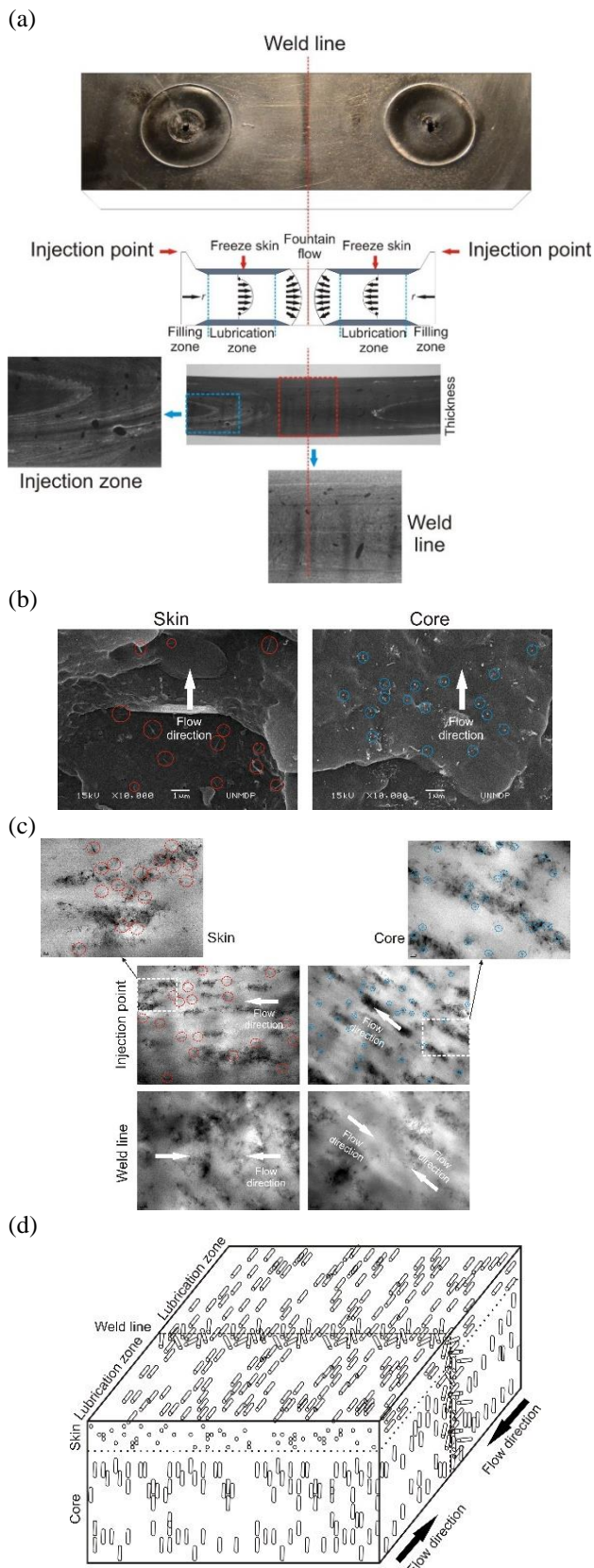


**Fig. 3.** Microstructural characterization of PP/MWCNT injected pieces. (a) Effects of the injection flow along the polymeric part observed by polarized light microscopy (PLM) (b) SEM images. (c) TEM images. (d) Scheme of the orientation of MWCNT at lubrication and weld line zone.

### Thermal resistance

Problems related to static charges can generate fires. That is the reason why thermogravimetric degradation tests were carried out under oxidative atmosphere. Results are shown in **Table 1**. MWCNTs improve thermal stability of PP, notably increasing  $T_{0.1}$ ,  $T_{0.5}$  and  $T_{max}$  in 35°C, 68°C, and 82°C respectively. It is observed that increasing in degradation temperatures is accompanied by a strong delay in material degradation. These improvements could be attributed to the barrier effect of MWCNT preventing the transport of degradation products from condensed to gaseous phase [36-38].

**Table 1.** Thermal and electrical properties of injected pieces.

Property	PP	PP/MWCNT		
		Injection point	Weld line	
Thermal	$T_{0.1}$ (°C)	285	320	
	$T_{0.5}$ (°C)	329	397	
	$T_{max}$ (°C)	342	424	
	char (%)	0.9	3.22	
Electrical	$\epsilon'$	2.09	73.84	44.34
	$\tan(\delta)$	0.007	0.101	0.373
	$\sigma_{ac}$ (S/cm)	$2.03 \times 10^{-11}$	$1.04 \times 10^{-8}$	$2.30 \times 10^{-8}$
	$\sigma_{dc}$ (S/cm)	$2.23 \pm 0.32 \times 10^{-14}$	$1.14 \pm 0.10 \times 10^{-10}$	$7.14 \pm 0.65 \times 10^{-9}$

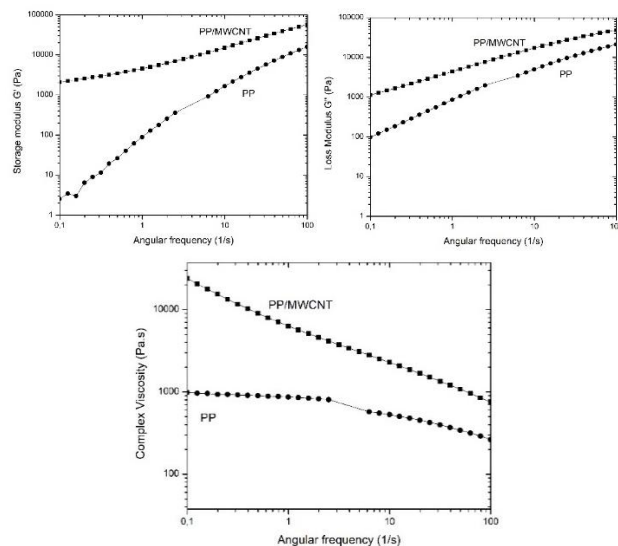


**Fig. 4.** Rheological properties of PP and PP/MWCNT.

### Rheological behavior

Rheological behavior was evaluated to infer the influence of particles on the internal microstructures and properties of polymer/MWCNT composites, since it can provide information about the percolated network structure, dispersion state of particles, and the interaction between particles and polymer matrix [3]. **Fig. 4** shows results. It is observed that PP/MWCNT exhibits higher viscosity with a strong shear thinning behavior (decreasing viscosity with increasing shear), while neat PP shows a Newtonian plateau at low frequencies. In the  $G'$  and  $G''$  vs. frequency plots a lower slope for PP/MWCNT is easily observed at low frequencies, especially for  $G'$ . It is been stated in literature that interconnected structures of non-isometric fillers

generate an apparent fluency similar to a solid material, that is seen in dynamic rheological measurements as lower slopes, tending to plateaus in  $G'$  or  $G''$  plots at low frequencies [39]. It could be therefore concluded that the percolation threshold has been overcome in injected PP/MWCNT parts.

### Electrical performance

Frequency dependence of the real electrical permittivity ( $\epsilon'$ ) and dielectric loss ( $\tan\delta$ ) curves of injected parts containing PP and PP/MWCNT composites, at room temperature, are shown in Fig. 5. PP parts present a typical insulation behavior, showing a low dielectric and loss permittivity values throughout the injected box. On the other hand, PP/MWCNT composite exhibits higher dielectric constant in all frequency range when compared with neat PP, and a relaxation process that changes depending on the zone of the box (injection point or weld line zone).

The higher dielectric constant in PP/MWCNT composites may be attributed to the formation of a huge number of tiny capacitors that arise from the conducting particles, which are separated by thin insulating layers. In this way, this nanocomposite may be consider as a capacitor with excellent characteristics for charge storage [40,41]. In addition, relaxation processes at low frequencies (typically below 100 Hz) could be attributed to a molecular or dipolar relaxation process (in the polymer chains), while at high frequencies they could be related to a space charge polarization, involving several mechanisms at the electrode-nanotube interfaces [42,43].

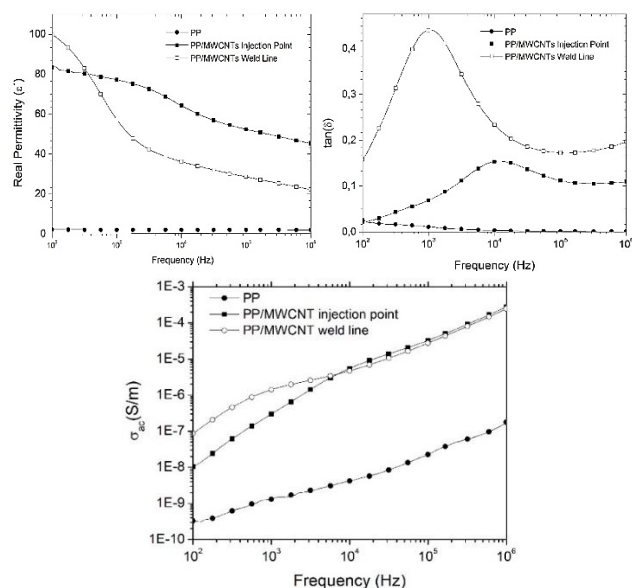


Fig. 5. Electrical and dielectrical properties of PP and PP/MWCNT composites as a function of frequency at room temperature.

The interfacial polarization process is likely attributed at the electrode-nanotube interface or Maxwell–Wagner–Sillars (MWS) relaxations [44]. In this process, the piling of charges at the interface causes large-scale field distortion or orientation of bound charge carriers, in contrast to the other types of polarizations (atomic, electronic, and dipolar) [45].

A simple model reported by Basu *et. al.*, [43] could be used to interpret the differences in relaxation frequencies related to the sample location. As previously said, the multiple CNT can be visualized as effective capacitors ( $C$ ) between the tubes in series with an effective resistor ( $R$ ) of carbon wall. The applied field,  $E$ , generates a voltage difference between successive tubes in the composite distant by  $d$ . The natural frequency of a single layer element of an analogous RC circuit is given by  $\omega_0 = 2\pi f = 1/RC$ . Then, the effective capacity,  $C$ , for multiples nanotubes is given by  $Q/nV$ , where  $n$  is the number of nanotubes and  $Q$  is the charge on each nanotube. So, solving  $\omega_0 = V^n/RQ$ . The better dispersion and random orientation of MWCNT observed in the weld line zone (see scheme in Fig. 3) may induce the formation of high number of micro-capacitors, increasing the capacity, the dielectric constant and decreasing the relaxation frequency in this zone [43,46]. On the other hand, the change on the distance between MWCNT,  $d$ , determines a difference in the relaxation frequency at electric conduction for the micro-capacitors and a peak in dielectric loss.

Fig. 5 also shows the frequency dependence of the electric conductivity for PP and PP/ MWCNT nanocomposite obtained at weld line and near the injection gate, at room temperature. The AC electrical conductivity,  $\sigma_{ac}$ , is higher in nanocomposites than in neat PP and it depends on the frequency, suggesting that CNT help to the increment of the electric charge transference at the interfaces. The composite shows a dependence of electrical conductivity with frequency and a property distribution throughout the injected part. In the original dielectric spectra, it is seen a mode one frequency dependence at 1 kHz and 10 kHz at the weld line and the injection point locations, respectively. Generally, the slow frequency mode observed in  $\sigma_{ac}(\omega)$  is typical of charge conductivity (at the weld line), while the faster frequency mode is reminiscent of that of induced polarization (at the gate point). Nevertheless, at low frequencies the relaxation processes is influenced by the DC conductivity [42]. For higher frequencies,  $\sigma_{ac}$  exhibits a slow increase which may be a sign of the highest volume concentration of MWCNT, also observed by Ahmad in alumina [47].

Table 1 shows the dielectric constant, loss tangent and AC (at 2500 Hz) and DC conductivity values of PP and PP/MWCNT composite, at room temperature. It can be observed that PP presents very low permittivity, conductivity DC and AC values, corresponding to those of an insulating material. Whereas the nanocomposite shows conductivity values 4 or 5 times higher than PP. It is also seen that, in samples extracted from the area affected by weld line, the DC conductivity is higher due to the favorable MWCNT orientation.

The DC conductivity is influenced by the formation of a network of MWCNT within the PP matrix [48]. It is known that DC may take place only when electrically conducting particles are in contact with each other and they cover a large distance and area in a network. Then, it can be in contact in a

point – spherical hard particles – or area – cylindrical particles. The contact area on the fillers allows the mobility of more charge carriers. Nanotubes allow large areas of contact depending on their relative orientation [49]. Their alignment through the use of electric [9,11] and magnetic [50] forces as well as flow-field mechanics [10] could increase electrical conductivity. Lanticse *et. al.* demonstrated that the electrical conductivity in the parallel direction to nanotubes is at least 4 orders of magnitude higher than the one in the perpendicular direction for 5 wt.% CNT [12]. In our injection molded composite, the high aspect ratio and the dispersion of MWCNT in the PP allow achieving particle-particle interactions at very low weight fraction of MWCNT, inducing electrical conductivities values typical of a percolated composite [51,52]. Distribution of properties in the molded parts is attributed to local differences in MWCNT orientation, amount and distribution induced by the complex thermomechanical environment developed inside the mold during processing.

### Mechanical and fracture performance

PP displays typical non-linear fragile behavior under three-point bending load. MWCNTs do not modify this behavior nor the maximum stress, but increase flexural modulus in 20% (Table 2). PP presents a brittle fracture surface while PP/MWCNT shows dissimilar failure mechanisms between skin and core: the skin presents a brittle fracture surface while the core is characterized by localized plastic deformation zones and smooth areas with no deformation (Fig. 6). It should be recalled here that flexural behavior is governed by the more elongated fiber which in this case corresponds to the samples' skin.

Table 2. Mechanical and fracture properties of injected pieces.

	PP		PP/MWCNT	
	Injection point	Weld line	Injection point	Weld line
$E_{flexural}$ (GPa)	2.5±0.1		2.8±0.1	
$\sigma_{flexural}$ (MPa)	91±1.5		90±3	
$K_{IC}$ (kN/m <sup>2</sup> )	2,6 ± 0,6	2,6	2,3 ± 0,3	2,1 ± 0,2
$G_{CP}$ (kJ.m <sup>2</sup> )	18,1 ± 4,3	18,7	8,4 ± 2	3,3 ± 0,4

PP/MWCNT behavior is the typical one of a micro-composite, probably due to the presence of agglomerates that decrease the interfacial ratio of the polymer-reinforcement minimizing the surface area of the exposed filler. Salvetat *et. al.* studied the behavior of CNTs in several composites and found that in order to genuinely take advantage of the high strength and modulus of the nanotubes, several conditions must be fulfilled, being the efficiency of load transfer the most important [53]. In fact, load transfer from matrix to CNTs plays a major role in the mechanical properties of these nanocomposites. If the adhesion between the matrix and the nanotubes is not strong enough to "withstand" high loads, then the benefits of the high tensile strength of the nanotubes are lost. Bikiaris stated that aggregates greater than 2-2.5% w/w decrease the tensile strength of PP/CNT nanocomposites: at low contents of nanoparticles, in pieces subjected to tensile efforts, load can be effectively transmitted to nanotubes

embedded in the PP matrix inducing an increase in tensile strength; at higher percentages of nanotubes, there is a greater formation of agglomerates in the matrix of PP that act as defects deteriorating the mechanical properties [21]. This last seems to occur in our composites.

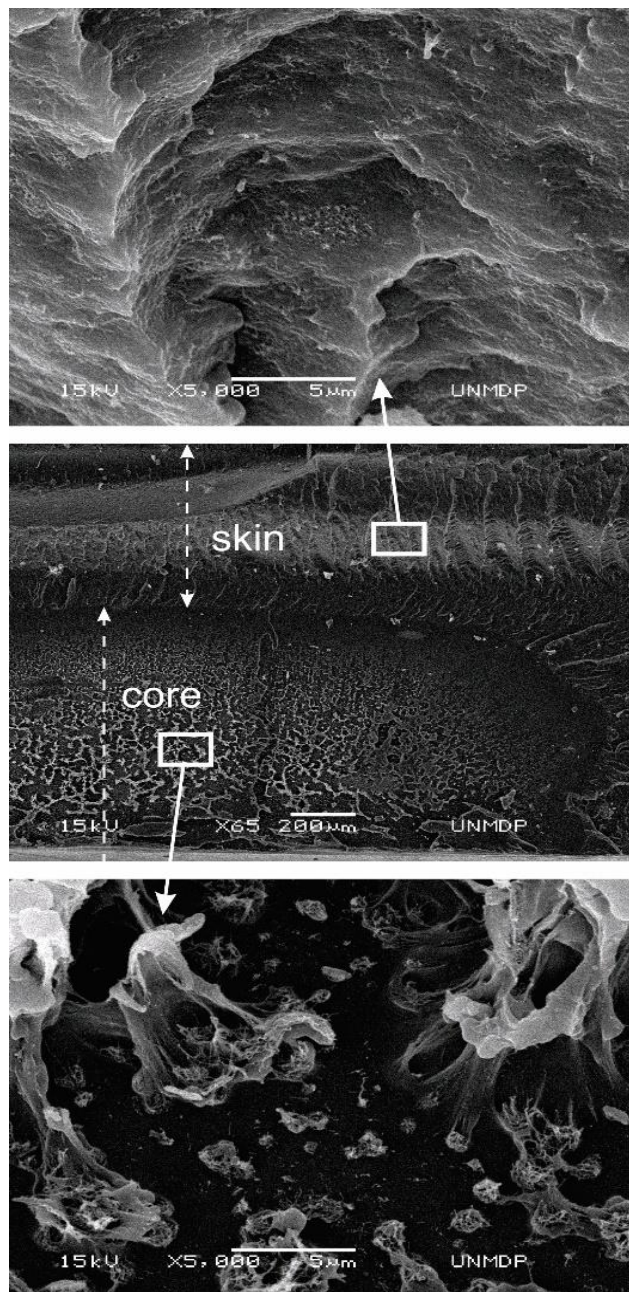


Fig. 6. SEM of post mortem fracture surfaces of PP/MWCNT tested under flexural load.

Typical load-deformation fracture curves are shown in Fig. 7 and fracture parameters depicted in Table 2. PP exhibits a fragile behavior, with quasi-linear load increasing up to a maximum where it falls to zero without further deformation. Incorporation of MWCNTs does not modify this behavior, but a decrease in the maximum load is observed accompanied with low deformation levels and catastrophic failure.

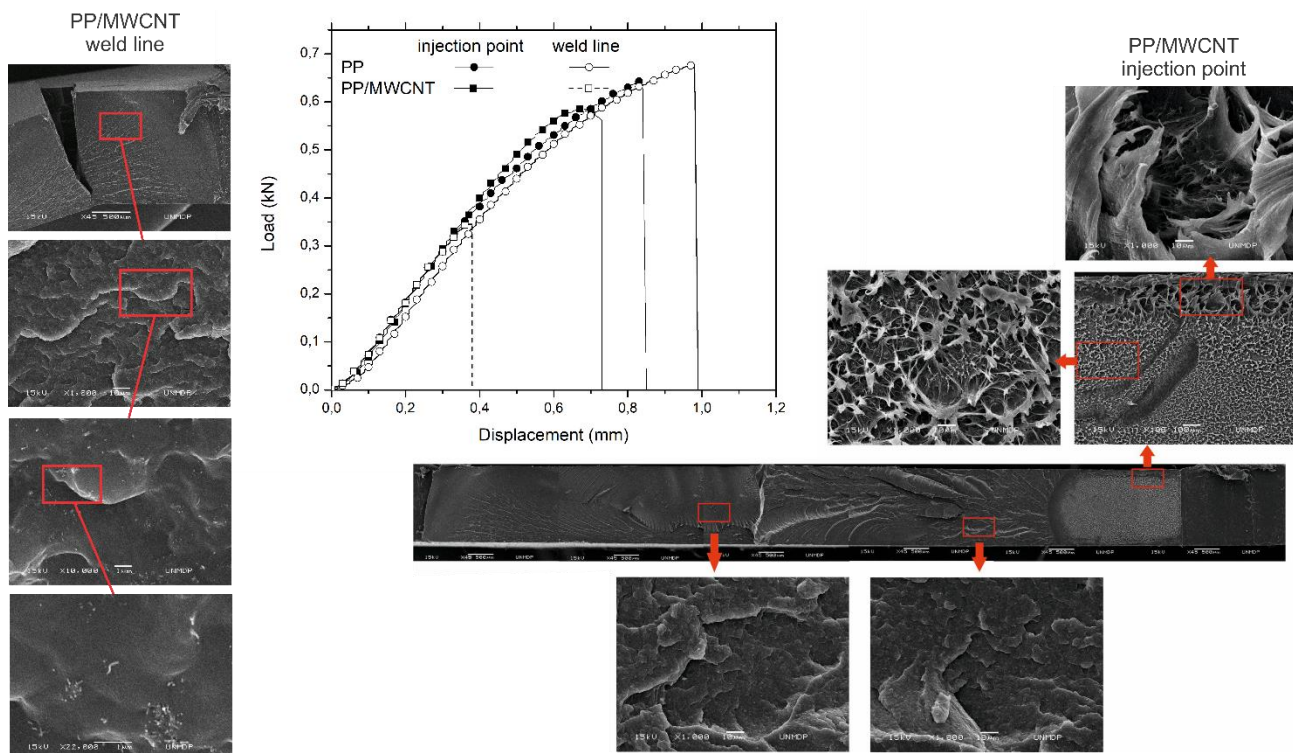


Fig. 7. Typical load-displacement curves for PP and PP/MWCNT samples obtained from different places of the injected pieces and fracture surfaces of PP/MWCNT samples observed by SEM.

Regarding fracture parameters, MWCNTs do not influence fracture initiation, similar values of  $K_{IC}$  are displayed (see **Table 2**). However, the energy absorbed during propagation decreases strongly for the nanocomposite, in particular for the specimens drawn from the weld line area. These differences between energy absorbed by PP/MWCNT samples near the injection point and those including the weld line can be explained by fracture surfaces examination. Nanocomposite samples exhibit two simultaneous deformation mechanisms in the area of the injection point: one of a ductile nature and one completely fragile (**Fig. 7**). While the fracture surface of the weld line area exhibits cleavage planes without any plastic deformation and nanotubes detached from the matrix. However, no matter the ability of MWCNT to induce a ductile fracture mechanism, it seems that agglomerates act as defects in the PP matrix diminishing the energy consumed during fracture propagation, when compared with pure PP.

#### Final discussion: processing-morphology-performance correlation

It should be pointed out here that the volumetric resistance measurements could be used to estimate the e-painting performance of the molded part. The painting efficiency is defined as the ratio between the deposited paint on a part surface and the paint lost during the painting process.

Nelson and Dahman showed that painting efficiency is almost equal to 1 (and equal to the painting efficiency corresponding to steel) for resistance values between

$10^5$ - $10^7$  ohm/cm, i.e., almost 100% of paint is efficiently transferred to the part surface [54]. These authors also reported that parts with resistivity values slightly larger than  $10^7$  ohm/cm (until  $10^9$  ohm/cm) still showed a very good painting efficiency. In **Fig. 8** our calculated values of volumetric resistance are shown along with the experimental data of transference painting efficiency vs. volumetric resistance obtained by Nelson and Dahman [54]. According to these data, painting efficiency would increase from 0.25 for neat PP parts (resistivity of  $\sim 10^{14}$  ohm/cm) to 0.7 (resistivity of  $\sim 10^9$  ohm/cm) for PP/MWCNT parts in weld line zone, what would lead to a very good painted surface. However, at the injection gate zone painting efficiency drops to 0.6 (resistivity of  $\sim 10^{10}$  ohm/cm), giving place to a final molded part with a paint gradient, i.e. more paint in some zones that in other zones of the same part. These differences in the electrical resistance values giving place to gradual painting throughout the parts illustrates the complexity of obtaining nanocomposites parts with homogeneous properties by injection molding.

Moreover, the relationships between electrical resistance and e-painting efficiency with  $G_c$  fracture parameter are also relevant (also shown in **Fig. 8**). It is seen that electrical resistivity increases (and e-painting decreases) as fracture propagation parameter  $G_c$  increases. This fact could be interpreted in terms of carbon nanotubes morphology/orientation: a 3D interconnected structure is optimal to obtain good electrical properties, but it seems not favorable in terms of fracture properties to induce

alternative toughness mechanisms. In summary, our results confirm that morphology developed during processing is determinant of the performance of final pieces.

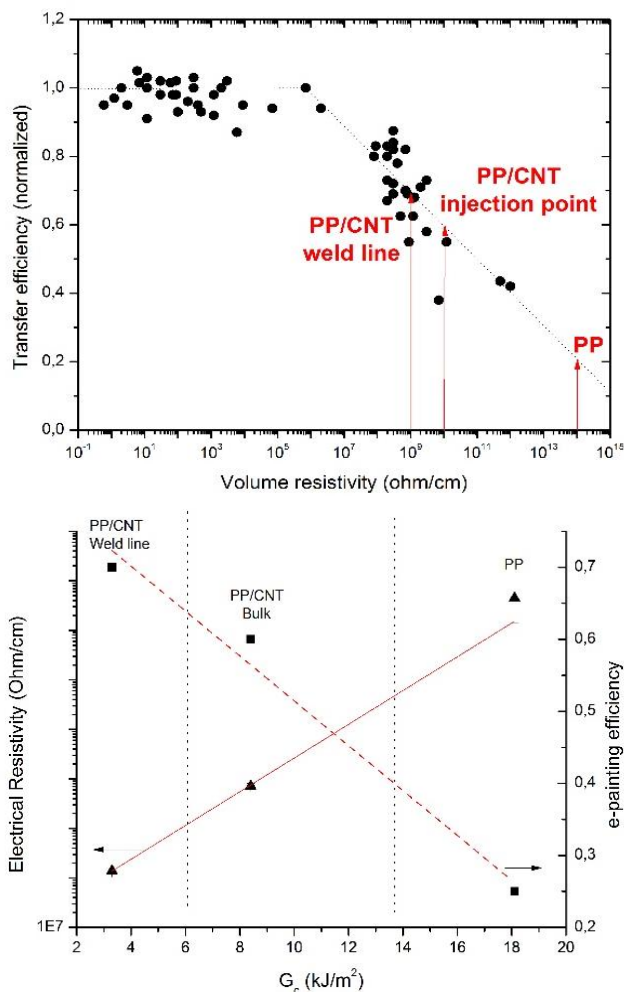


**Fig. 8.** Comparison of paint transfer efficiency of PP and PP/MWCNT at different locations of injection molded boxes with data from Nelson and Dahman [54], and its relationship with the fracture propagation parameter  $G_c$ .

## Conclusion

Through this work the influence of MWCNT particles on the performance of real complex injected PP parts was explored. It was found that PP/MWCNT molding parts present lower shrinkage in the main axes in comparison with PP ones, resulting in injected parts of better aesthetic quality. Regarding morphology, PP/MWCNT molding parts present agglomerates – despite the presence of compatibilizer – and an anisotropic morphology of nanotubes (inside the agglomerates and individually) with an orientation gradient along the thickness in the area near the injection point. The welding line is a strong heterogeneity where the nanotubes are oriented in a more random way due to the complex velocity field of the flow. MWCNT were beneficial in terms of thermal resistance. PP/MWCNT presents a markedly better thermal stability than pure PP, due to a barrier effect of the nanotubes that

prevent the transport of degradation products from condensed to gaseous phase.

It was observed that the incorporation of 3 wt.% MWCNT increases the dielectric constant and AC and DC conductivity, principally at the weld line due to the more efficient conductive filler distribution. Also, interfacial polarization processes known as Maxwell–Wagner–Sillars were generated by particles influenced by the filler orientation. From a practical point of view, reasonably good DC conductivity values were reported in PP/MWCNT composites allowing its use as an additive for e-painting. However, electrical properties were higher at the weld line, which can produce defects during the painting process of molded parts.

In terms of mechanical performance, MWCNTs generate only a slight increase in conventional mechanical properties. MWCNTs do not change fracture initiation value ( $K_{IC}$ ), but fracture propagation values ( $G_{IC}$ ) fall abruptly especially for the samples drawn from the area of the welding line, due to the heterogeneous orientation and particle dispersion of the material that induces different fracture mechanisms in the pieces. From a structural point of view, the latter is not desirable for any technological market.

It was found a correlation between electrical and fracture properties: electrical resistivity increases as fracture propagation parameter  $G_c$  increases due to the MWCNT 3D interconnected structure, which is optimal for electrical properties but not favorable to generate alternative toughness mechanisms. Also, the distribution of properties throughout the injection molded parts was attributed to differences in MWCNT orientation, amount and distribution induced by the complex thermo-mechanical environment developed inside the mold during processing.

In other words, MWCNT modification improved several aspects of injected pieces as aesthetic quality, thermal stability, electrical conductivity and stiffness. However, the energy absorbed during fracture propagation is deteriorated, fact that should be taken in mind when applications include severe mechanical solicitations. It is then evident that it results necessary to find an alternative way to obtain parts with the aesthetic finish required by the market without adding processing steps, without deteriorating the fracture performance.

## Acknowledgements

Authors would like to thank CONICET; University of Mar del Plata and ANPCyT for financial support.

## Conflicts of interest

There are no conflicts to declare.

## Keywords

Injection molding, dielectric properties, mechanical properties, fracture behaviour, structure-property relations

Received: 23 September 2020

Revised: 1 December 2020

Accepted: 2 December 2020

## References

1. Julien, C.; *Materials Science and Engineering: B*, **1990**, 6, 9.
2. Jogi, B.F.; Sawant, M.; Kulkarni, M. et al.; *J. Encapsulation Adsorpt. Sci.*, **2012**, 02, 69.
3. Ballav, N.; Biswas, M.; *Mater. Sci. Eng.: B*, **2006**, 129, 270.
4. Gupta R, Kennel E, Kim K-J. *Polymer Nanocomposites Handbook*. CRC Press Taylor & Francis Group, <https://www.crcpress.com/Polymer-Nanocomposites-Handbook/Gupta-Kennel-Kim/p/book/9780849397776> (2009, accessed 3 August 2018).
5. Lee, S.H.; Cho, E.; Jeon, S.H.; et al.; *Carbon*, **2007**, 45, 2810.
6. Sun, W.; Mo, Z.; *Mater. Sci. Eng.: B*, **2013**, 178, 527.
7. Sandler, J.K.W.; Kirk, J.E.; Kinloch, I.A.; et al.; *Polymer*, **2003**, 44, 5893.
8. Kilbride, B.E.; Coleman, J.N.; Fraysse, J.; et al.; *J. Appl. Phys.*, **2002**, 92, 4024.
9. Celzard, A.; McRae, E.; Deleuze, C.; et al.; *Phys. Rev. B*, **1996**, 53, 6209.
10. Balberg, I.; Binenbaum, N.; *Phys. Rev. B*, **1983**, 28, 3799.
11. Carmona, F.; El Amarti, A.; *Phys. Rev. B*, **1987**, 35, 3284.
12. Lantice, L.J.; Tanabe, Y.; Matsui, K.; et al.; *Carbon*, **2006**, 44, 3078.
13. Kalaitzidou, K.; Fukushima, H.; Drzal, L.T.; *Compos. Sci. Technol.*, **2007**, 67, 2045.
14. Fujiyama, M.; Wakino, T.; *Int. Polym. Process.*, **1992**, 7, 159.
15. Motlagh, G.H.; Hrymak, A.N.; Thompson, M.R.; *J. Polym. Sci. Pol. Phys.*, **2007**, 45, 1808.
16. Weber, M.; Kamal, M.R.; *Polym. Compos.*, **2004**, 18, 726.
17. Dani, A.; Ogale, A.A.; *Compos. Sci. Technol.*, **1996**, 56, 911.
18. Arjmand, M.; Apperley, T.; Okoniewski, M.; et al.; *Carbon*, **2012**, 50, 5126.
19. Hattum, F.W.J.; Van Leer C.; Viana, J.C.; et al.; *Plast. Rubber Compos.*, **2006**, 35, 247.
20. Bao, H.D.; Guo, Z.X.; Yu, J.; *Polymer*, **2008**, 49, 3826.
21. Bikiaris, D.; *Materials (Basel)*, **2010**, 3, 2884.
22. Lin, X.; Tian, J.W.; Hu, P.H.; et al.; *J. App. Polym. Sci.*, **2016**, 133.
23. Nguyen-Tran, H.D.; Hoang, V.T.; Dom V.T.; et al.; *Materials*, **2018**, 11.
24. Pötschke, P.; Mothes, F.; Krause, B.; et al.; *Polymers*, **2019**, 11, 189.
25. Reinholds, I.; Roja, Z.; Zicans, J.; et al.; *IOP Conf Ser: Mater Sci Eng*, **2015**, 77, 012013.
26. Villmow, T.; Pegel, S.; Pötschke, P.; et al.; *Compos. Sci. Technol.*, **2008**, 68, 777.
27. Wu, M.; Shaw, L.L.; *J. Power Sources*, **2004**, 136, 37.
28. Abbasi, S.; Carreau, P.J.; Dourdour, A.; *Polymer*, **2010**, 51, 922.
29. Patti, A.; Russo, P.; Acierino, D.; et al.; *Compos. Part B-Eng.*, **2016**, 94, 350.
30. Pegel, S.; Pötschke, P.; Petzold, G.; et al.; *Polymer*, **2008**, 49, 974.
31. Williams, G.C.; Kc and Gc at slow speeds for polymers. In: *Fracture Mechanics Testing Methods for Polymers, Adhesives and Composites*. Elsevier, Oxford, UK, **2001**.
32. Adams, M.J.; Williams, D.; Williams, J.G.; *J. Mater. Sci.*, **1989**, 24, 1772.
33. Seo, M.K.; Park, S.J.; *Chem. Phys. Lett.*, **2004**, 395, 44.
34. Bay, R.S.; Tucker, C.L.; *Polym. Compos.*, **1992**, 13, 317.
35. Gamba, M.M.; Pouzada, A.S.; Frontini, P.M.; *Polym. Eng. Sci.*, **2009**, 49, 1688.
36. Yang, J.; Lin, Y.; Wang, J.; et al.; *J. Appl. Polym. Sci.*, **2005**, 98, 1087.
37. Marosfői, B.B.; Szabó, A.; Marosi, G.; et al.; *J. Therm. Anal. Calorim.*, **2006**, 86, 669.
38. Zhao, Y.; Ding, X.; Jiao, Q.; et al.; Thermal Stability of Polypropylene/Carbon Nanotube Composites. *China Plastics*.
39. Dealy, J.M.; Wissbrun, K.F.; *Melt Rheology and Its Role in Plastics Processing: Theory and Applications*, Springer, Netherlands, **1999**.
40. Shri Prakash, B.; Varma, K.B.R.; *Compos. Sci. Tech.*, **2007**, 67, 2363.
41. Ramajo, L.; Castro, M.S.; Reboredo, M.M.; *J. Mater. Sci.*, **2009**, 45, 106.
42. Ramajo, L.; Castro, M.S.; Reboredo, M.M.; *Compos. Part A-App. S.*, **2007**, 38, 1852.
43. Basu, R.; Iannacchione, G.S.; *Appl. Phys. Lett.*, **2008**, 92, 052906.
44. Karahaliou, P.K.; Kerasidou, A.P.; Georga, S.N.; et al.; *Polymer*, **2014**, 55, 6819.
45. Tsangaris, G.M.; Kouloumbi, N.; Kyvelidis, S.; *Mater. Chem. Phys.*, **1996**, 44, 245.
46. Ramajo, L.A.; Cristóbal, A.A.; Botta, P.M.; et al.; *Compos. Part A-App. S.*, **2009**, 40, 388.
47. Ahmad, K.; Pan, W.; Shi, S-L.; *Appl. Phys. Lett.*, **2006**, 89, 133122.
48. Vavouliotis, A.; Fiamegou, E.; Karapappas, P.; et al.; *Polym. Compos.*, **2010**, 31, 1874.
49. Endo, M.; Kim, Y.A.; Hayashi, T.; et al.; *Carbon*, **2001**, 39, 1287.
50. Xu, Y.; Higgins, B.; Brittain, W.J.; *Polymer*, **2005**, 46, 799.
51. Barrau, S.; Demont, P.; Peigney, A.; et al.; *Macromolecules*, **2003**, 36, 5187.
52. Valentini, L.; Puglia, D.; Frulloni, E.; et al.; *Compos. Sci. Technol.*, **2004**, 64, 23.
53. Salvétat, J-P.; Bonard, J-M.; Thomson, N.H.; et al.; *Appl. Phys. A.*, **1999**, 69, 255.
54. Nelson, B.; Dahman, S.; Colorable Thermoplastic Compounds for Electrostatic Painting Applications. In: ANTEC Proceedings, **2000**.